

Deliverable Data					
Deliverable number	D5.3 (D14)				
Deliverable name	Design of an adjustable beam focusing system for PW lasers				
Work Package	WP5 (task 5.2b)				
Lead WP/deliverable beneficiary	CNRS/CNRS				
Type and dissemination level Report, public					
Deliverable status					
Submitting author	B. Le Garrec				
Verified (WP leader)	P. Audebert				
Approved (Coordinator)	V. Bagnoud				
Due date of deliverable	31/05/2025				



## **Table of Contents**

A	۱bo	out THRILL1
E	Σxe	ecutive summary2
	00	cument History4
1		Introduction and objectives5
2	<u>)</u>	Step-by-step design of the on-axis 3-mirror telescope
3	3	Paraxial calculations of the 3-mirror telescopic zoom8
3	3.1	Condition 1
3	3.2	Condition 2
3	3.3	Condition 311
3	3.4	Condition 4
3	3.5	Consequences of conditions 1 & 2
3	8.6	Condition 5
4	ļ	3 <sup>rd</sup> and 5 <sup>th</sup> order spherical aberration
5	,	Unobscured off-axis design
6	;	C-C-D zoom design
7	•	Experimental results
8	3	Conclusion5
9	)	References6
ı	_is	st of figures
_		e 1: the 3-mirror telescopic configurations to be considered, from top to bottom D-C-D, D-C-C, C-D and C-C-C
_		e 2: the 3-mirror system with the successive images and their respective distances labelled ording to the mirror vertices
li	ne	e 3: because of conditions 1 & 2, the possible domain for the zoom range is between the 2 red s (for the 4 possible 3-mirror configurations starting with D-C or C-C). There are no solutions for figurations when the second mirror $M_2$ is divergent (configurations starting with D-D & C-D) 12
_		e 4: example of on-axis propagation through a D-C-C system (not to scale). Ray tracing made



figure 5: top: same as figure 4 when the beam is off-axis through a D-C-C system (not to scale). Ray tracing made with VirtualLab Fusion []. Bottom: off-axis 140-mm beam (at 820 nm) excentered 210 mm in the D-C-D zoom system at median position. The scale along x is multiplied by 2 for better reading. Ray tracing made with VirtualLab Fusion []
igure 6: un-obscured off-axis situation for configurations C-C-D
igure 7: the ratio $h_{1min}/\phi$ for y = -1.5, -2, -2.5, -3 (red, green, blue, black) with the respective x ranges (condition 1). A high y value reduces the off-axis
Figure 8: principle of the CCD design with available mirror $R_1$ = - 305 mm, $R_2$ = 610 mm, $R_3$ = 800 mm. The system is set for $d_{12}$ = - $d_{23}$ so $d_{13}$ = 0 (top figure and medium line of table 2), then for long focal length (middle figure and top line of table 2) and short focal length (bottom figure and bottom line of table 2). Figures are not to scale.
igure 9: final design of the C-C-D zoom for a medium range focal length of 1.56 m and a back focal length of 1.6 m. Mirror mounts are cut out kinematic types to minimize the off-axis distance that is given on figure 7. $M_1$ is fixed; translations for $M_2$ and $M_3$ are parallel to each other and to the incident beam axis. Final focal spot is fixed
Figure 10: wavefront error (WFE) for left to right a beam $\Phi 8.5$ excentred 10mm, $\Phi 8.5$ excentred 5mm and $\Phi 10$ excentred 6mm for the medium position $d_{12} = -d_{23} = 607$ mm (calculated with VLF software[6])
igure 11: an exemple of wavefront calculated by Atmos for the zoom for 2 wavelengths (532 and 820 nm) with a 8.5 mm diameter beam excentred 6 mm2
igure 12:experimental set-up (not to scale) showing the $3^{rd}$ zoom with the maximum range. $M_2$ is moving 115 mm and $M_3$ 442 mm. Both translations are parallel
figure 13: focal spots recorded for the 8 positions of mirrors $M_2$ and $M_3$ according to Table 34
igure 14: left, focal spot area square roots at half maximum (blue curve) and at 1/e <sup>2</sup> (red curve) as a function of the zoom focal length and right, the focal spot normalized intensity as a function of the zoom focal length4

#### **Disclaimer**

This document is part of the deliverables from the project THRILL, which has received funding from the European Union. Views and opinions expressed are however those of the author(s) only and do not necessarily reflect those of the European Union or the European Commission. Neither the European Union nor the granting authority can be held responsible for them.



#### About THRILL

The THRILL project deals with providing new schemes and devices for pushing forward the limits of research infrastructures (RI) of European relevance and ESFRI landmarks. To do so, the project partners have identified several technical bottlenecks in high-energy high-repetition-rate laser technology that prevent it from reaching the technical readiness level required to technically specify and build the needed devices, and guaranteeing sustainable and reliable operation of such laser beamlines at the partnering RIs. Advancing the technical readiness of these topics is strategically aligned with the long-term plans and evolution of the ESFRI landmarks FAIR, ELI (-BL) and Eu-XFEL, and RI APOLLON, bringing them to the next level of development and strengthening their leading position.

The project is focused and deliberately restricted to three enabling technologies, which require the most urgent efforts and timely attention by the community: high-energy high-repetition-rate amplification, high-energy beam transport and optical coating resilience for large optics. To reach our goals, the major activity within THRILL will be organized around producing several prototypes demonstrating a high level of technical readiness. Our proposal is addressing not yet explored technical bottlenecks - such as transport over long distances of large-aperture laser beams via relay imaging using all-reflective optics - and aims at proposing concrete steps to increase the performances and effectiveness of the industrial community through the co-development of advanced technologies up to prototyping in operational environments.

The project is not only pushing technology, it is also offering an outstanding opportunity to train a qualified work force for RIs and industry. With this in mind, the structure of THRILL promotes synergetic work, fast transfer to industry and integrated research activities at the European level. Access to the RIs will be granted as in-kind contribution.



## **Executive summary**

As part of WP5 of THRILL on advanced laser beam control, this study focuses on the design and validation of a three-mirror telescopic zoom system using spherical mirrors to meet the stringent optical requirements for laser-driven electron acceleration at petawatt-class laser facilities.

The primary objective is to vary the focal length continuously without displacing the final focal spot, while respecting laser-induced damage thresholds that prohibit beam compression. Multiple optical configurations were analyzed, and a 1/5-scale mock-up constructed at the Apollon facility enabled validating the design. Experimental measurements of aberrations closely matched theoretical predictions, confirming the accuracy and reliability of the optical model.

Key challenges addressed in the design include:

- Maintaining high beam quality with minimal spherical aberration across the zoom range.
- Avoiding central beam obscuration by adopting off-axis mirror configurations.
- Ensuring mechanical feasibility in a vacuum environment with large-diameter laser beams.
- A step-by-step geometrical design method was developed to evaluate both on-axis and offaxis systems, adhering to the following constraints:
- No beam obscuration at any zoom position.
- A real final image over the entire zoom range.
- Minimum mirror beam size maintained (≥95% of the incoming beam).
- Fixed final focal spot position throughout zooming.
- Numerical aperture maintained between f/15 and f/20.

Among the eight possible mirror arrangements (combinations of converging and diverging mirrors), four configurations were found viable. The C-C-D (convergent-convergent-divergent) setup was identified as the optimal solution, offering a balance of compactness, low aberration, and mechanical practicality.

Three reduced-scale systems were designed, built, and tested:

- 1. D-C-D: Very compact, but with limited zoom range and mechanical complexity.
- 2. D-C-C: Offers multiple aberration minimization points, but is excessively long.
- C-C-D: Best overall performance, allowing compact implementation with excellent beam quality.

The C-C-D configuration, when implemented in an off-axis layout, successfully avoids





obscuration while maintaining optical performance.

In conclusion, this work demonstrates that reflective zoom systems using spherical mirrors can be precisely engineered through geometrical analysis to deliver high-quality, variable-focus laser beams suitable for advanced applications like laser-plasma electron acceleration, all while operating within laser damage thresholds and mechanical constraints.





## **Document History**

Version	Date	Changes	Reviewer/ contributor
V1 – first draft	4/03/2025		LULI
V1 – reviews	30/05/2025		LULI
V1.2	12/05/2025	Formatting	GSI
V1.3	10/06/2025	Executive summary	LULI



## 1 Introduction and objectives

Both the size of the focal spot and the Rayleigh range of laser beams are increasing with the focal length of a focusing system. Telescopic zoom systems made of three spherical mirrors can be designed for such purpose. A telescopic zoom system made of three spherical mirrors has been designed for the purpose of electron acceleration with lasers at LULI's Apollon facility [1]. This system is based on a telescope with 3 or 4 mirrors, the distances of which can be varied continuously. We are constrained by laser damage considerations which prevent us from reducing the dimension of the incident laser beam. It is possible to get a continuous range of focal lengths when translating the second mirror such that the final focal length will vary from 1 to 4 (zoom ratio 4x) and that the final focal spot will not move. When dealing with on-axis mirrors, we will get a central obscuration and the next step will be to go off-axis such that no obscuration will occult the beam propagation.

After a first attempt to design such system based on simple "a priori" parameters, a general algebraic theory has been investigated and shows that there are always solutions with no spherical aberration. When all mirrors are placed off-axis to avoid obscuration of the beam, it is possible to show that there are still solutions that minimize aberrations. When changing the distance between the mirrors, we can change the focal length of the system while the final focal spot is fixed. I have built and tested three zoom systems based on different solutions and I have been able to show that there are simple alignment procedures for generating a fixed focal spot over the zoom range.

The mirror zoom problem is complex and despite an abundant literature, the case of reflective systems is restricted to telescopes with a first (and large) converging mirror. The 3-mirror problem has already been investigated by Korch in 1973 [2] but his very nice and compact set of equations doesn't tell you what to do to find the possible solutions. I have decided to follow a step-by-step analysis based on geometrical considerations.



# 2 Step-by-step design of the on-axis 3-mirror telescope

At the Apollon facility as in the case of all high-energy lasers, laser beams are fairly well collimated with a divergence much less than 100  $\mu$ rads, and the object is at infinity. Moreover, there is no aperture stop anywhere on the beam path because all the optical components are much larger than the beam. The beam profile is close to a flat-top or high-order super-gaussian in some image-relay planes. The goal of the study is to find what are the zoom solutions that minimize spherical aberration (when considering on-axis systems) for a given numerical aperture over a given zoom range. These solutions are then extended to off-axis systems. The conclusion is that a final wavefront aberration of much less than  $\lambda/4$  can be reached when the numerical aperture is between f/15 and f/20.

There are 9 parameters to be considered when looking at 3-mirror telescopes:

- radii of curvature: R1, R2, R3,
- distances between mirrors: d12, d23,
- beam heights at the mirror surfaces: h1, h2, h3,
- 1 distance between the fixed mirror and the final image (the focal spot),

My approach is made of the following steps:

- Find all possible designs with three on-axis spherical mirrors assuming that:
  - There is no total obscuration of the beam (1st condition)
  - The system M1-M2 is not afocal (2nd condition)
  - The final image is real over the zoom range or in other words, avoid any virtual final image (3rd condition)
  - The size of the beam on any mirror cannot be less than 95% of the incoming beam
     (4th condition related to the laser damage fluence with a 10% margin)
- The final focal spot is located at a fixed position
- Minimize beam heights for unobscured off-axis design with ex-centered beams.

For practical reasons related to our experimental set-up, I have decided "a priori" that:

- The numerical aperture will be small enough and between f/15 and f/20,
- The magnification of the 2nd and 3rd mirrors will be close to or greater than  $\pm 2$  such that the final focal length of the system will be at minima 4 to 10 times the focal length of the first mirror,
- Based on some mechanical considerations and the fact that the final system will be under

Version 1.3, Date 10/06/2025



vacuum, the mirrors size should not be too large, at least much less than 1m and if possible, less than 0.5 m.

When considering a three-mirror telescopic system, there are eight different possible configurations based on the type of mirror: convergent (C) or divergent (D):

- D-C-D, very compact
- D-C-C, not compact
- · C-C-D, compact
- C-C-C, very long
- D-D-D has no final real image
- D-D-C, very low magnifications = short final focal length & large beam on M3
- C-D-D has no final real image
- C-D-C, very low magnifications = short final focal length & large beam on M<sub>3</sub>

There are 4 possible configurations to be considered when the second mirror  $M_2$  is convergent (see Fig. 1). In my first paper [3], I was only considering the first configuration (D-C-D) that was extrapolated from an inverse Galilean 2-mirror telescope with concentric or nearly-concentric mirrors because it was always possible to find an on-axis design such that the spherical aberration equals zero.

Notation and sign convention are according to analytical geometry [4] that is, distances from left to right are positive-from right to left negative; distances measured upwards, positive - downwards, negative; angles measured counterclockwise, positive - clockwise, negative. Objects are labelled  $A_i$ ; images  $A'_{i,;}$  mirror positions  $M_i$ ; their respective center of curvature  $C_i$  and radius of curvature  $R_i$ ; beam heights  $h_i$ ; distances to vertices  $x_i$ ; distances between mirrors i and i+1  $d_{ii+1}$ ; magnifications  $\beta_i$ .

For reflection, image refractive index n' and object refractive index n are such that:

$$n'_i = (-1)^i \& n_i = (-1)^{i+1}$$
 (1)



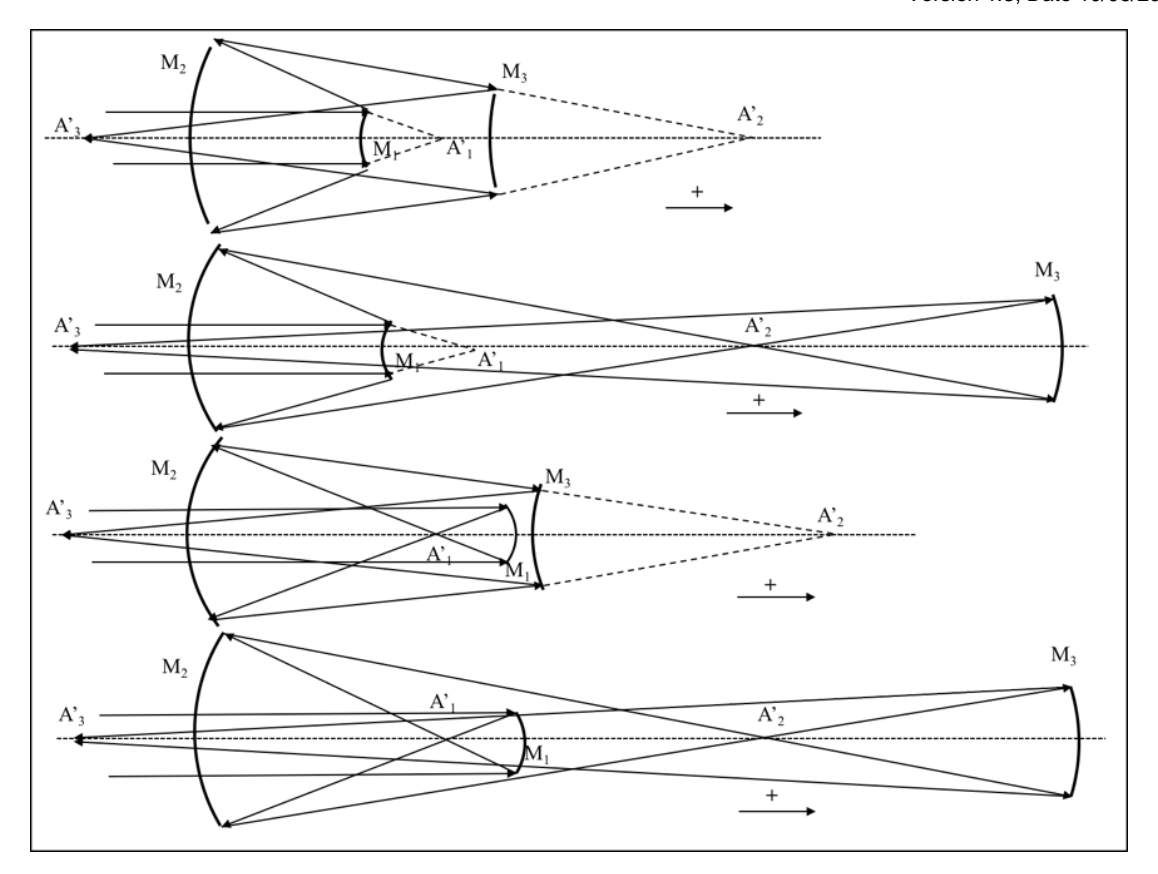


Figure 1: the 3-mirror telescopic configurations to be considered, from top to bottom D-C-D, D-C-C, C-C-D and C-C-C.

# 3 Paraxial calculations of the 3-mirror telescopic zoom

There are three distances to be considered: between mirrors  $M_1$  and  $M_2$ ,  $M_2$  and  $M_3$  and distance from mirror  $M_3$  to the final image  $A'_3$  (therefore the focal spot of our laser). The paraxial equations for the three mirrors  $M_i$  are respectively with i=1, 2, 3:

$$\frac{(-1)^i}{x'_i} = \frac{(-1)^{i+1}}{x_i} + \frac{[(-1)^i - (-1)^{i+1}]}{R_i}$$
 (2)

Distances between mirrors are such that (cf. Fig.2):

$$x'_1 = d_{12} + x_2 \quad \& \quad x'_2 = d_{23} + x_3$$
 (3)

Focal lengths are defined as:

$$f'_{i} = (-1)^{i} \frac{R_{i}}{2} \tag{4}$$

The focal length of the system can be expressed as the product of the focal length of the 1<sup>st</sup> mirror and magnifications of the 2<sup>nd</sup> and 3<sup>rd</sup> mirrors:

$$f'_{1+2+3} = f'_{1}\beta_{2}\beta_{3} \tag{5}$$



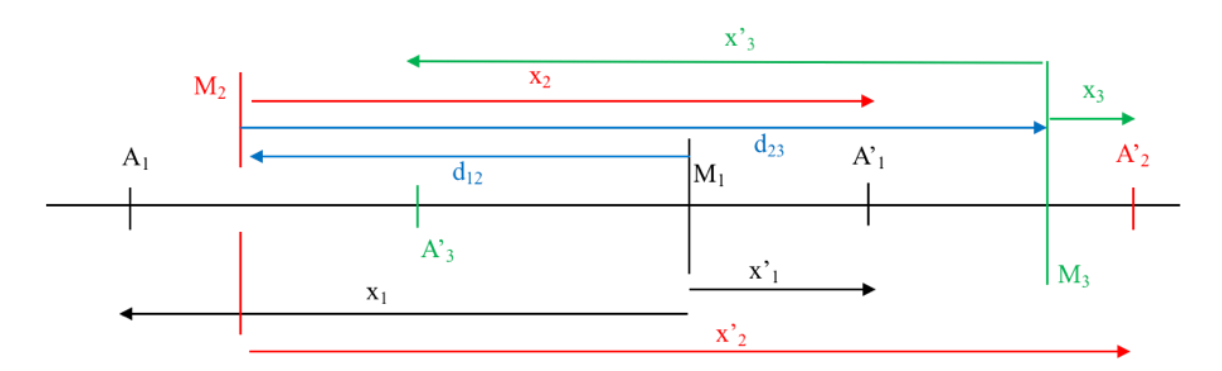


Figure 2: the 3-mirror system with the successive images and their respective distances labelled according to the mirror vertices.

If both mirrors  $M_2$  and  $M_3$  are moving for the zoom function, then  $M_1$  can be fixed and the object being at infinity,  $A'_3$  will be fixed. This means that the distance from  $M_1$  to  $A'_3$  is constant when  $d_{12}$  varies. The distance  $M_1A'_3$  simply depends on  $d_{12}$ ,  $d_{23}$  and  $x'_3$  (the back focal length):

$$\overline{A'_1 A'_3} = \overline{A'_1 M_1} + \overline{M_1 M_2} + \overline{M_2 M_3} + \overline{M_3 A'_3} = -x'_1 + d_{12} + d_{23} + x'_3$$
 (6)

$$\overline{A'_1 A'_3} = \overline{A_2 A'_2} + \overline{A'_2 A'_3} = \overline{A_2 A'_2} + \overline{A_3 A'_3} = x'_2 - x_2 + x'_3 - x_3 \tag{7}$$

(3) can be written as:

$$x'_{2} = f'_{2}(1 - \beta_{2}) \& x_{2} = f'_{2}(1 - \frac{1}{\beta_{2}})$$
 (8)

$$x'_3 = f'_3(\beta_3 - 1) \& x_3 = f'_3(\frac{1}{\beta_2} - 1)$$
 (9)

From (6), (7), (8) and (9), one gets:

$$d_{12} + d_{23} + x'_3 - x'_1 = f'_2 \left(\frac{1}{\beta_2} - \beta_2\right) + f'_3 \left(\beta_3 - \frac{1}{\beta_3}\right)$$
 (10)

In our case, object is at infinity:

$$x'_1 = \frac{R_1}{2} = -f'_1 \tag{11}$$

(10) reduces to:

$$d_{12} + d_{23} + x'_{3} = \overline{M_{1}A'_{3}} = -f'_{1} + f'_{2} (1/\beta_{2} - \beta_{2}) + f'_{3} (\beta_{3} - 1/\beta_{3})$$
(12)

The left term of (12) is simply the distance from the first mirror  $M_1$  to the final image  $A'_3$ : if I want this distance to be constant whatever the values of  $d_{12}$  and  $d_{23}$ , then the final image is fixed. According to (9), I can decide what magnification I want and get  $x'_3$  (that is finally the



back focal length of the system). By substituting for  $x'_3$  from (9) into (12), I can find the relation between  $d_{12}$  and  $d_{23}$ .

At that stage, I am introducing the following reduced variables:

- $x = -d_{12}/R_1$ , the ratio of the distance from M<sub>1</sub> to M<sub>2</sub> to the radius of curvature of M<sub>1</sub>,
- $y = R_2/R_1$ , the ratio of the radius of curvature of  $M_2$  to the radius of curvature of  $M_1$ ,
- $z = d_{23}/R_2$ , the ratio of the distance from M<sub>2</sub> to M<sub>3</sub> to the radius of curvature of M<sub>2</sub>,
- $w = R_3/R_2$ , the ratio of the radius of curvature of  $M_3$  to the radius of curvature of  $M_2$ .

From relations (2) and (3):

$$x'_{2} = \left(\frac{R_{2}}{2}\right) \frac{(1+2x)}{(1+2x-y)} \tag{13}$$

$${\chi'}_{3} = \left(\frac{R_{3}}{2}\right) \frac{(1+2x)(1-2z)+2yz}{1+2x-(2z+w)(1+2x-y)} \tag{14}$$

$$\beta_2 = -\frac{x_{2}}{x_2} = -\frac{y}{1+2x-y} \tag{15}$$

$$\beta_3 = -\frac{x'_3}{x_3} = -w \frac{1+2x-y}{1+2x-(2z+w)(1+2x-y)} \tag{16}$$

The focal length of the system (5) can be expressed as:

$$f'_{1+2+3} = -\left(\frac{R_1}{2}\right) \frac{yw}{1+2x-(2z+w)(1+2x-y)} \tag{17}$$

The beam heights on the mirrors are equal to:

$$h_2 = h_1(1 - 2 d_{12}/R_1) = h_1(1 + 2x)$$
(18)

And with (13):

$$h_3 = h_2(1 - 2d_{23}/x'_2) = h_1(1 + 2x - 2z(1 + 2x - y))$$
(19)

#### 3.1 Condition 1

Full occultation by M<sub>1</sub> of the beam reflected by M<sub>2</sub> occurs when:

$$d_{12} = R_2 - \frac{R_1}{2}$$
 or  $x = y - \frac{1}{2}$  (20)

The condition to avoid full occultation reads:

$$x > 0$$
 then  $x < y - \frac{1}{2}$  and  $x < 0$  then  $x > y - \frac{1}{2}$  (21)



#### 3.2 Condition 2

The 2-mirror system M<sub>1</sub>-M<sub>2</sub> is afocal when:

$$d_{12} = (R_1 - R_2)/2 \text{ or } 2x = y - 1$$
 (22)

The condition to avoid afocal reads:

$$x > 0 \text{ then } x > \frac{y-1}{2} \text{ and } x < 0 \text{ then } x < \frac{y-1}{2}$$
 (23)

#### 3.3 Condition 3

The final image is real when the distance from mirror M<sub>2</sub> to mirror M<sub>3</sub> is such that:

$$d_{23} > x'_2 - \frac{R_3}{2} = \left[ R_2 \left( \frac{1+2x}{1+2x-y} \right) - R_3 \right] / 2 \tag{24}$$

$$R_2 > 0$$
 then  $2z + w > \left(\frac{1+2x}{1+2x-y}\right)$  and  $R_2 < 0$  then  $2z + w < \left(\frac{1+2x}{1+2x-y}\right)$  (25)

#### 3.4 Condition 4

Let's consider first the case when the beam size  $\Phi_3$  is the same on  $M_3$  and  $M_1$  ( $\Phi_1$ ). This size is connected to (19) and (25) and finally depends on the sign of w:

$$w > 0 \text{ then } \frac{h_3}{h_1} > 1 \text{ and } z < \left(\frac{x}{1 + 2x - y}\right)$$
 (26)

$$w < 0 \text{ then } \frac{h_3}{h_1} < -1 \text{ and } z > \left(\frac{1+x}{1+2x-y}\right)$$
 (27)

So for  $\Phi_3/\Phi_1 > 0.9$ , (26) and (27) become:

$$w > 0 \ then \ \frac{h_3}{h_1} > 0.95 \ and \ z < \left(\frac{x + 0.05}{1 + 2x - y}\right)$$
 (28)

$$w < 0 \text{ then } \frac{h_3}{h_1} < -0.95 \text{ and } z > \left(\frac{x + 0.95}{1 + 2x - y}\right)$$
 (29)



### 3.5 Consequences of conditions 1 & 2

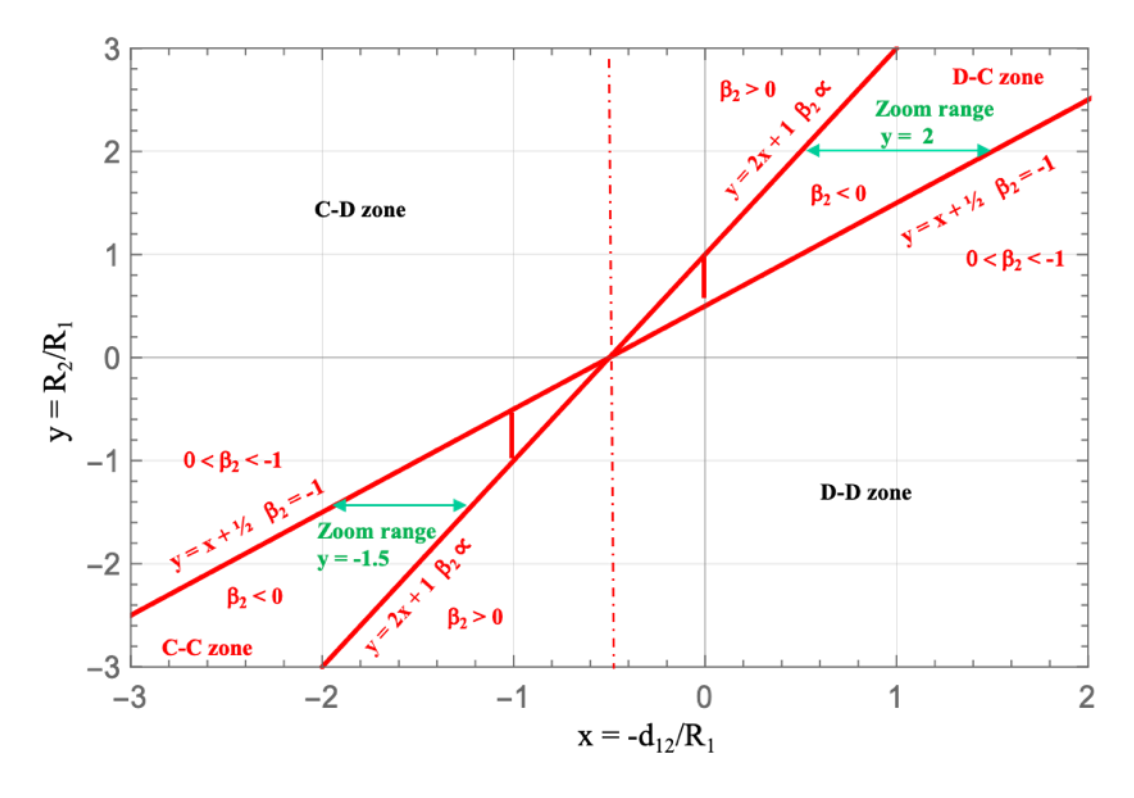


Figure 3: because of conditions 1 & 2, the possible domain for the zoom range is between the 2 red lines (for the 4 possible 3-mirror configurations starting with D-C or C-C). There are no solutions for configurations when the second mirror  $M_2$  is divergent (configurations starting with D-D & C-D).

#### 3.6 Condition 5

The final formulae (12) for getting a fixed focal spot can be written a different way because both  $x'_3$ ,  $\beta_2$  and  $\beta_3$  depend on x, y, z and w through (14, 15, 16). With the reduced variables  $x = -d_{12}/R_1$ ,  $y = R_2/R_1$ ,  $z = d_{23}/R_2$ ,  $w = R_3/R_2$  and introducing the constant  $K = M_1A'_3$ , I finally get the following  $2^{nd}$  degree equation:

$$z^{2} + zB(x, y, w) + C(x, y, w) = 0$$
(30)

with:

$$B(x, y, w) = \left(w - \frac{x}{y} - \frac{K}{yR_1} - \frac{1+2x}{2(1+2x-y)}\right)$$
(31)

and:

$$C(x,y,w) = \left(\frac{1+2x}{1+2x-y} - w\right) \left(\frac{x}{2y} + \frac{K}{2yR_1}\right) - w \frac{1+2x}{4(1+2x-y)}$$
(32)

The  $2^{nd}$  degree equation finally gives the relation between z and x ( $d_{23}$  and  $d_{12}$ ) when the other variables are set. Because z is always positive, there is only one solution.



## 4 3rd and 5th order spherical aberration

The wavefront aberration of a centered system consisting of any number of refractive (or reflective) spherical surfaces can be calculated as in Born and Wolf [5] or equal to the Seidel B-term in Korch [2]. The wavefront aberration is equal to the path length difference between the real ray and the paraxial ray along the paraxial ray and can be expressed as follows:

$$\Delta_{5th} = \sum_{i} n'_{i} \Delta_{i} = \sum_{i} \frac{h_{i}^{4} Q_{ix}^{2}}{8} \left( \frac{1}{n'_{i}x'_{i}} - \frac{1}{n_{i}x_{i}} \right) + \frac{h_{i}^{6} Q_{ix}^{2}}{16R_{i}^{2}} \left( \frac{1}{n'_{i}x'_{i}} - \frac{1}{n_{i}x_{i}} \right) + \frac{h_{i}^{6} Q_{ix}^{3}}{16} \left( \frac{1}{n'_{i}x'_{i}^{2}} - \frac{1}{n_{i}^{2}x_{i}^{2}} - \frac{1}{n_{i}^{2}x_{i}^{2}} \right)$$
(33)

with the Abbe's invariant:

$$Q_{ix} = n'_i \left( \frac{1}{x'_i} - \frac{1}{R_i} \right) = n_i \left( \frac{1}{x_i} - \frac{1}{R_i} \right)$$
 (34)

$$\Delta_{5th} = -\Delta_1 + \Delta_2 - \Delta_3 \tag{35}$$

$$\Delta_{5th} = -\frac{h_1^4 Q_{1x}^2}{4R_1} - \frac{h_1^6 Q_{1x}^2}{8R_1^3} + \frac{h_1^6 Q_{1x}^3}{16} \left(\frac{1}{{x'}_1^2} - \frac{1}{x_1^2}\right) + \frac{h_2^4 Q_{2x}^2}{4R_2} + \frac{h_2^6 Q_{2x}^2}{8R_2^3} + \frac{h_2^6 Q_{2x}^3}{16} \left(\frac{1}{{x'}_2^2} - \frac{1}{x_2^2}\right) - \frac{h_3^4 Q_{3x}^2}{4R_3} - \frac{h_3^6 Q_{3x}^2}{8R_3^3} + \frac{h_2^6 Q_{2x}^2}{4R_3} + \frac{h_2^6 Q_{2x}^2}{16} \left(\frac{1}{x_1^2} - \frac{1}{x_2^2}\right) - \frac{h_3^4 Q_{3x}^2}{4R_3} - \frac{h_3^6 Q_{3x}^2}{8R_3^3} + \frac{h_3^6 Q_{2x}^2}{4R_3} + \frac{h_3^6 Q_{$$

$$\frac{h_3^6 Q_{3x}^3}{16} \left( \frac{1}{x r_3^2} - \frac{1}{x_3^2} \right) \tag{36}$$

With:

$$Q_{1x} = \left(\frac{1}{x_1} - \frac{1}{R_1}\right); Q_{2x} = \left(\frac{1}{x_2'} - \frac{1}{R_2}\right); Q_{3x} = \left(\frac{1}{x_3} - \frac{1}{R_3}\right)$$
(37)

$$h_2 = h_1 (1 + d_{12} \left( \frac{1}{x_1} - \frac{2}{R_1} \right)) \tag{38}$$

$$h_3 = h_2 (1 + d_{23} \left( \frac{1}{x_2} - \frac{2}{R_2} \right)) \tag{39}$$

$$\Delta_{3th} = \sum_{i} n'_{i} \Delta_{i} = \sum_{i} \frac{n'_{i} h_{i}^{4} Q_{ix}^{2}}{4R_{i}} = -\frac{h_{1}^{4} Q_{1x}^{2}}{4R_{1}} + \frac{h_{2}^{4} Q_{2x}^{2}}{4R_{2}} - \frac{h_{3}^{4} Q_{3x}^{2}}{4R_{3}}$$
(40)

#### 3rd order spherical aberration when the object is at infinity

 $x = -d_{12}/R_1$ ,  $y = R_2/R_1$ ,  $z = d_{23}/R_2$  and  $w = R_3/R_2$ ,

$$\Delta_{3th} = h_1^4 \left[ -\frac{1}{4R_1^3} + \frac{(1+2x)^2(1+2x-2y)^2}{4R_2^3} - \frac{\{1+2x-2z(1+2x-y)\}^4}{4R_3^3} \left\{ \frac{2w(1+2x-y)}{1+2x-2z(1+2x-y)} - 1 \right\}^2 \right]$$
(41)

Formulas (36) and (40) are explicitly calculated within the ranges given by conditions 1 to 5:

- in an Excel spreadsheet when the object is at a given distance or at infinity,
- with Mathematica in order to plot the wavefront distortions as a function of any of the reduced variables x, y, z & w,
- with a ray-tracing software like VirtualLab Fusion [6] or Atmos [7] for plotting the off-axis wavefront error (WFE) and the decomposition in Zernike polynomials.



A very important result is that for a given numerical aperture, formula (41) will give you a given  $\Delta_{3h}$  that scales as h: if distances are multiplied by 2, you get  $2\Delta_{3h}$  and if distances are divided by 2 you get  $\Delta_{3h}$  /2. That's why I have built and tested 3 different zooms at reduced scale [8].

At first the calculations are made for a centered system and the beam radius is larger than the expected off-axis beam + the off-axis height (necessary for avoiding obscuration), cf. fig. 5a & 5b. The min & max values of the beam height on  $M_1$ ,  $M_2$  and  $M_3$  are calculated in the Excel spreadsheet with formulas (18, 19) and condition 1.

As explained above, different configurations have been tested, considering a scale-1 system that could be used for the 140-mm petawatt  $F_2$  beam of Apollon assuming a numerical aperture between f/15 and f/20 and mirror diameters not exceeding 600 mm:

- DCD; the initial and most compact solution that was published in 2021 [3]. See figure
   5b. For a 140-mm beam, the system fits in a 15-m long box.
- DCC; because there are two "zeros" of the 3<sup>rd</sup> order aberration formula (41) over the focal range but the overall system is quite long. For a 140-mm beam, the system needs more than a 20-m long box.
- CCD; the "best compromise solution" that was optimized for a the 120-mm petawatt beam F<sub>2</sub> at Apollon's facility. For a 140-mm beam, the system fits in a 12-m long box. This was published in 2023 [8].

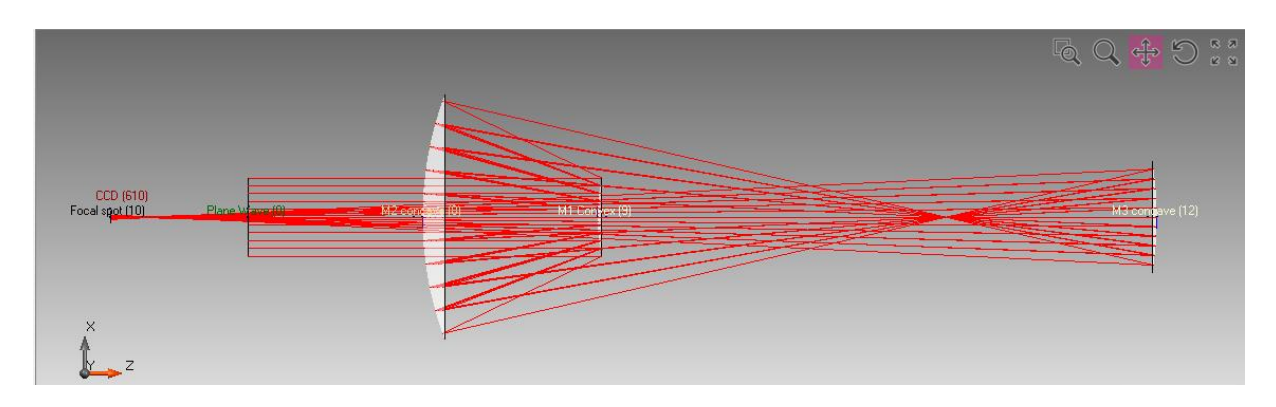


Figure 4: example of on-axis propagation through a D-C-C system (not to scale). Ray tracing made with VirtualLab Fusion [6].



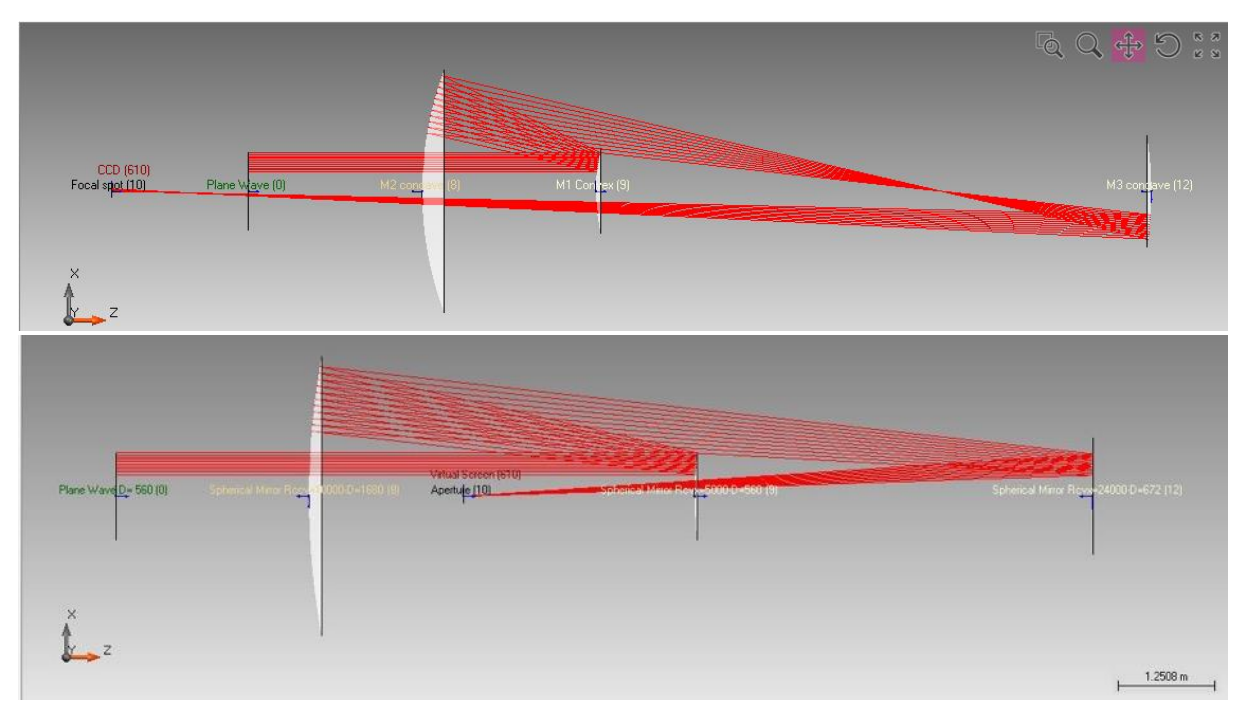


Figure 5: top: same as figure 4 when the beam is off-axis through a D-C-C system (not to scale). Ray tracing made with VirtualLab Fusion [6]. Bottom: off-axis 140-mm beam (at 820 nm) excentered 210 mm in the D-C-D zoom system at median position. The scale along x is multiplied by 2 for better reading. Ray tracing made with VirtualLab Fusion [6].

## 5 Unobscured off-axis design

The beam cannot be centered on the axis because its central part will be reflected backwards. Going off-axis is a necessary condition but one has to know the minimum beam height for avoiding obscuration by  $M_1$  of the beam reflecting by  $M_2$ . And then the same problem will occur with the beam reflected by  $M_3$  that can be obscured by  $M_1$  or  $M_2$ . In fact, this depends on the chosen configuration; there is no real difficulty to solve this issue, it's only geometrical considerations that I have detailed in my second paper [8]. Here, I am considering only the configuration which minimizes the off-axis distance.

For configurations starting with C-C, there is a minimum height on  $M_1$  such that the beam reflected by  $M_3$  is not obscured by  $M_2$  or  $M_1$  (see Fig. 6).



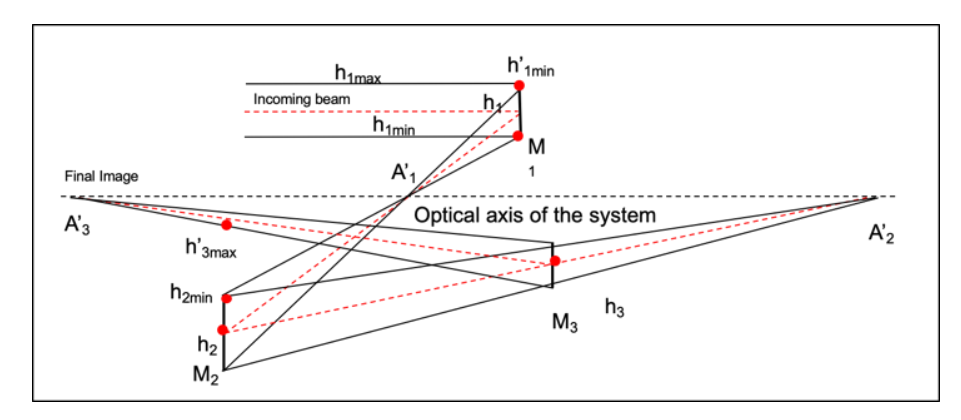


Figure 6: un-obscured off-axis situation for configurations C-C-D.

For the C-C-D configuration, the maximum height of the beam reflected by  $M_3$  in the plane of  $M_2$  ( $h'_{3max}$ ) must be smaller than the minimum height on  $M_2$  ( $h_{2min}$ ):  $h'_{3max} > h_{2min}$ . From formulas (18, 19) and with  $\Phi$  the diameter of the beam, we can write:

$$h'_{3\text{max}} = h_{3\text{max}} (x'_{3} + d_{23})/x'_{3} \& h_{1\text{max}} = h_{1\text{min}} + \Phi$$
 
$$h'_{3\text{max}} = h_{1\text{max}} ((1+2x)(w+2z)-z(4z+5w)(1+2x-y))/2w = \zeta(h_{1\text{min}} + \Phi)$$
 With: 
$$\zeta = (1+2x-2z(1+2x-y)+2z(1+2x-(2z+w)(1+2x-y))/w$$

For the C-C-D configuration, we finally get the condition for non-obscuration as illustrated Figure 7:

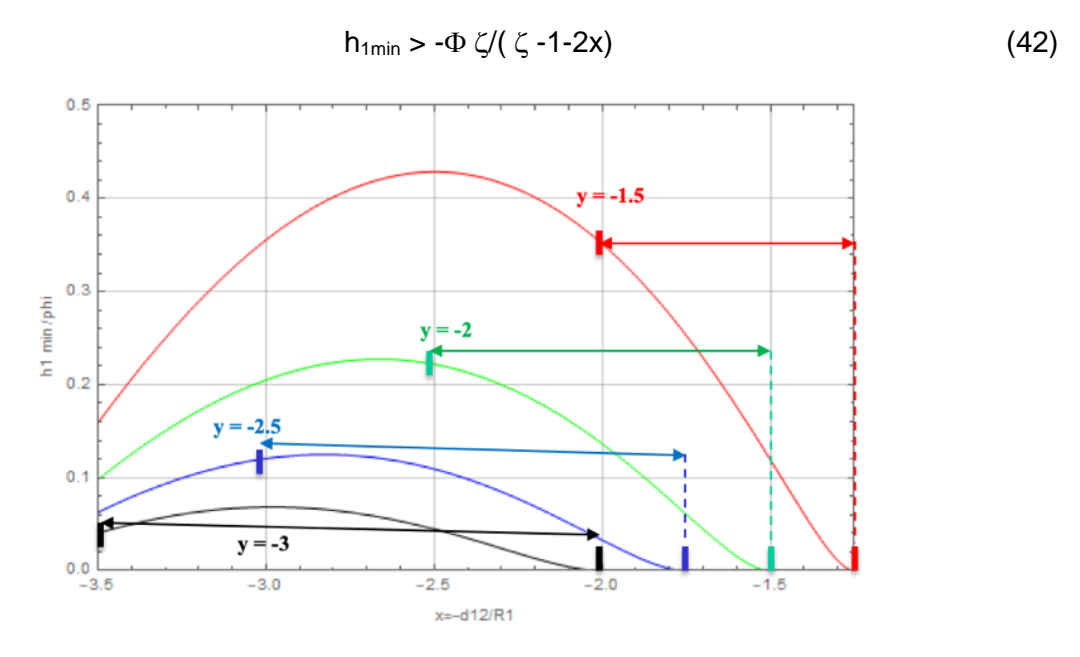


Figure 7: the ratio  $h_{1min}/\phi$  for y = -1.5, -2, -2.5, -3 (red, green, blue, black) with the respective x ranges (condition 1). A high y value reduces the off-axis

## 6 C-C-D zoom design

Both the choice of the configurations and the choice of the radii of curvature of the mirrors were



driven by the mirrors that were available at the lab at LULI or that I could buy "off-the-shelf" at low price (between \$50 and \$ 300 for 2-inch mirrors with silver protected or aluminium protected coatings). I have built and tested three zoom systems based on 3 different configurations: D-C-D (as ref. [2]), D-C-C (because there are two zeros for spherical aberration within the zoom range) and C-C-D.

**Table 1**: parameters of the three mirrors. Signs of distance and radii of curvature are according to **Figure 2**.

Config.	R <sub>1</sub> (m)	R <sub>2</sub> (m)	R <sub>3</sub> (m)	у	w	x <sub>min</sub> , x <sub>max</sub> (m)	$z(x_{min})$ $z(x_{max})$	f' <sub>1+2+3</sub> (X <sub>min</sub> ) (X <sub>max</sub> )	
C-C-D	-0.305	0.610	0.8	-2	1.31	-2.39 -1.90	0.57 1.21	2.32 0.79	
Diameter	2"	2"	50 mm						
Ref.	49-602	32-818	87-687	Supplier: Edmund Optics					
Price (€)	154	154	80						

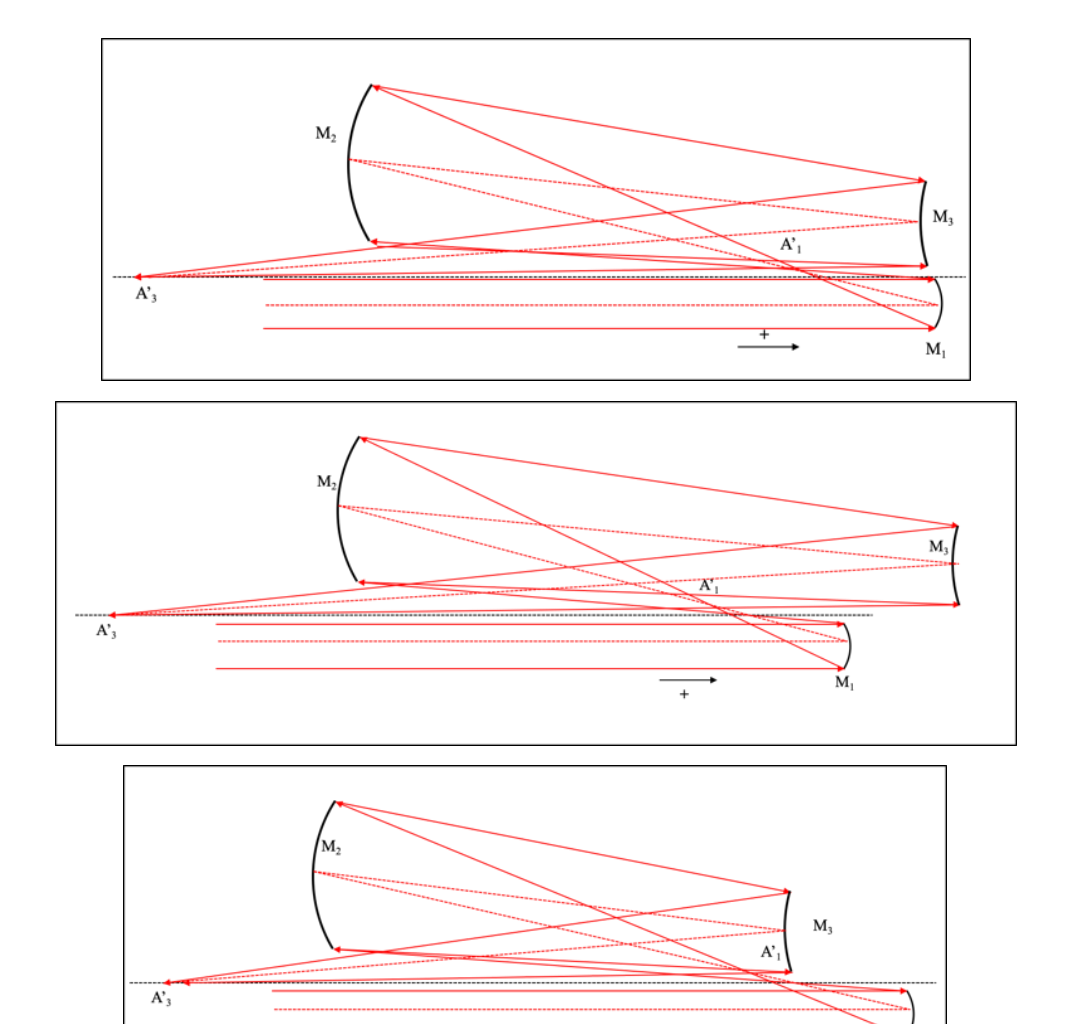


Figure 8: principle of the CCD design with available mirror  $R_1$ = - 305 mm,  $R_2$ = 610 mm,  $R_3$ = 800 mm.



The system is set for  $d_{12}$ = -  $d_{23}$  so  $d_{13}$ = 0 (top figure and medium line of table 2), then for long focal length (middle figure and top line of table 2) and short focal length (bottom figure and bottom line of table 2). Figures are not to scale.

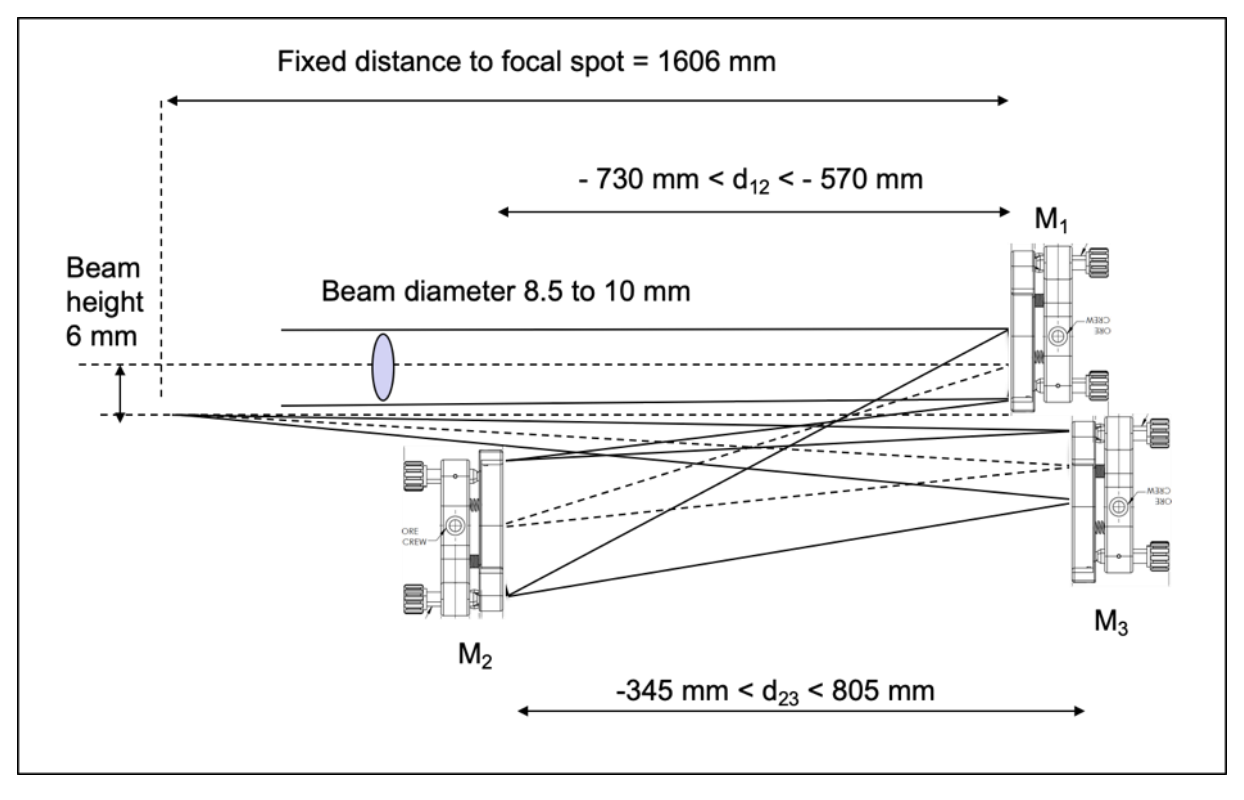


Figure 9: final design of the C-C-D zoom for a medium range focal length of 1.56 m and a back focal length of 1.6 m. Mirror mounts are cut out kinematic types to minimize the off-axis distance that is given on figure 7.  $M_1$  is fixed; translations for  $M_2$  and  $M_3$  are parallel to each other and to the incident beam axis. Final focal spot is fixed.

Table 2: results of calculation with Atmos [9] for a 8.5 mm beam size excentred 6 mm. The zoom range is such that the beam size on  $M_3$  is not less than 90% of the incoming beam size (condition 4).

d <sub>12</sub> (mm)	d <sub>23</sub> (mm)	f' <sub>123</sub> (m)	WFE (λ=532 nm)	Strehl Ratio
-570	803.3	2.32	0.24	0.91
-580	738.3	2.06	0.23	0.92
-607	607	1.56	0.19	0.94
-710	369.5	0.77	< 0.01	1
-730	345	0.69	0.04	1



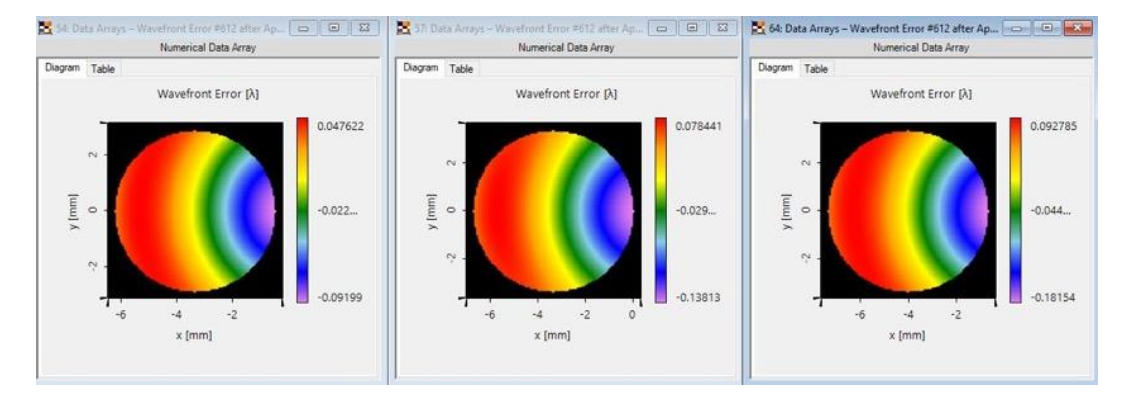
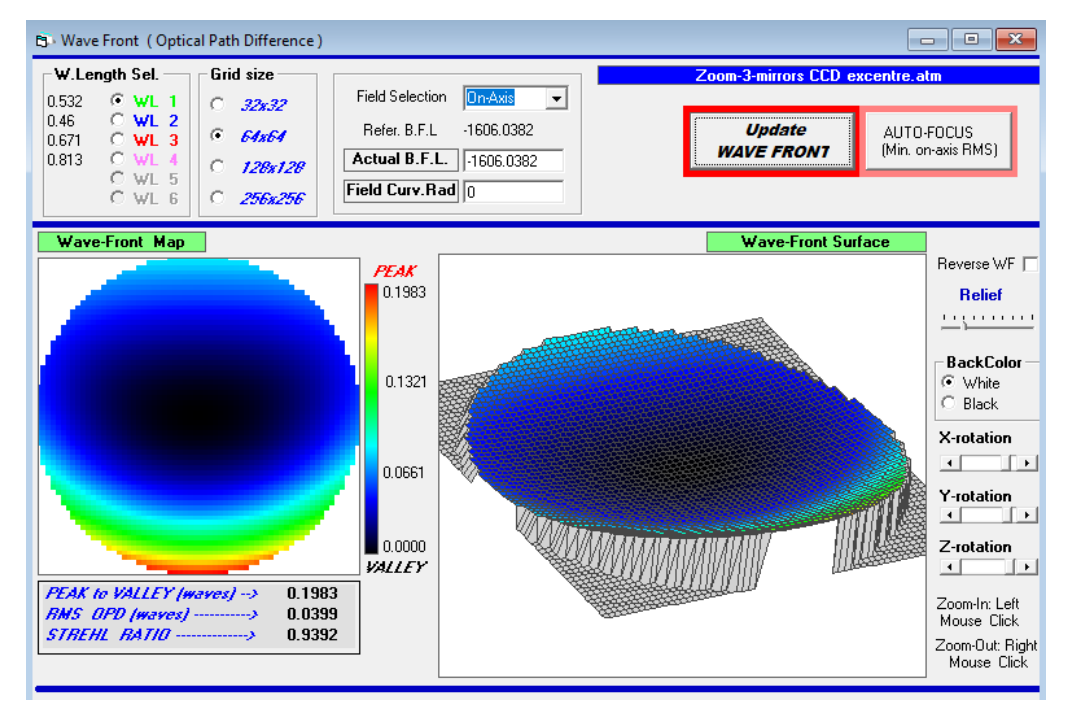


Figure 10: wavefront error (WFE) for left to right a beam  $\Phi$ 8.5 excentred 10mm,  $\Phi$ 8.5 excentred 5mm and  $\Phi$ 10 excentred 6mm for the medium position  $d_{12} = -d_{23} = 607$  mm (calculated with VLF software[6])





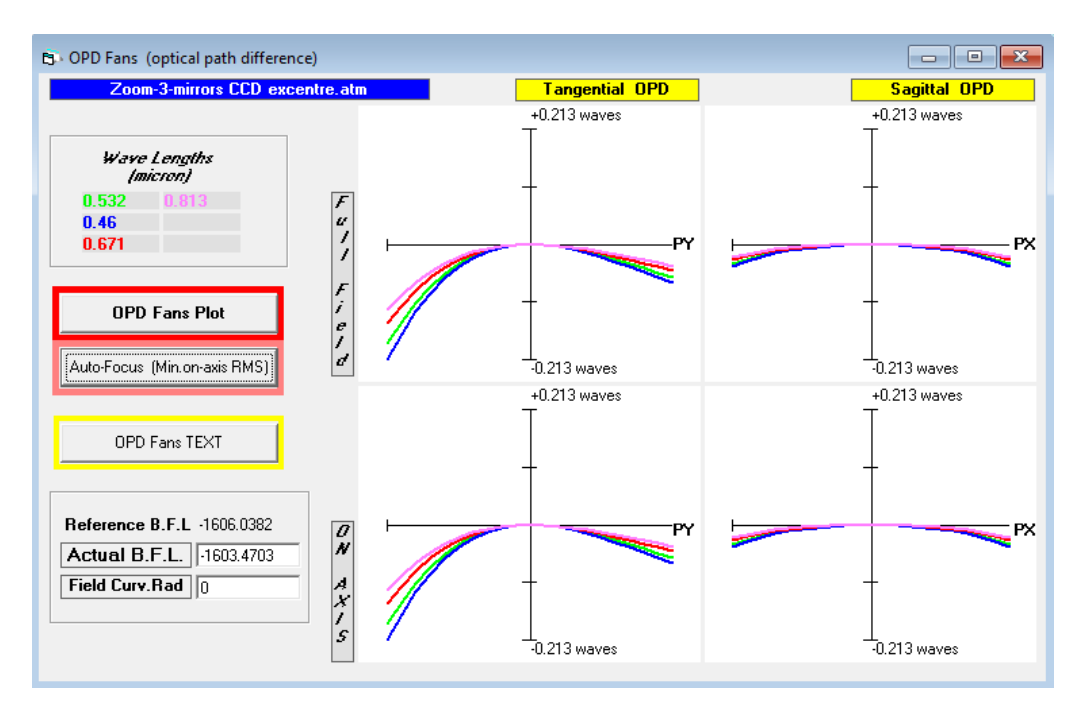


Figure 11: an example of wavefront calculated by Atmos for the zoom for 2 wavelengths (532 and 820 nm) with a 8.5-mm-diameter beam excentred 6 mm.

## 7 Experimental results

The experimental set-up is made of two parts: a simple collimator and the 3-mirror zoom system. Both fit on a 2 m x1.2 m breadboard. The collimator is made of a collimated laser diode delivering 5 mW at 532nm, a microscope objective X10 and NA=0.25, a 30- $\mu$ m pinhole and a corrected doublet lens, diameter 80 mm & f=150 mm. Two variable apertures are located on the beam path such that the final collimated beam diameter can be tuned from 1 to 25 mm. At 1-mm collimated beam, alignment is made by auto-collimating mirrors M<sub>1</sub>, M<sub>2</sub> and M<sub>3</sub> such that all beams are in an horizontal plane. Because all mirrors are much larger than necessary, beams are located off-axis on one edge of each mirror and the tip-tilt mounts are of the "open-back-plate" for minimizing obscuration. All three experimental set-ups have shown that the translation of M<sub>2</sub> and M<sub>3</sub> can be parallel. At first, the distance d<sub>12</sub> is set to a given value and d<sub>23</sub> is tuned such that the distance from M<sub>1</sub> to the focal spot is equal to the calculated "K" parameter. The CCD camera [9] is protected from ambient light with a ND3 neutral density filter. The CCD camera has 1280 pixels x 960 pixels and a 3.75  $\mu$ m spatial resolution. The input beam diameter was set to 9 ± 0.5 mm.



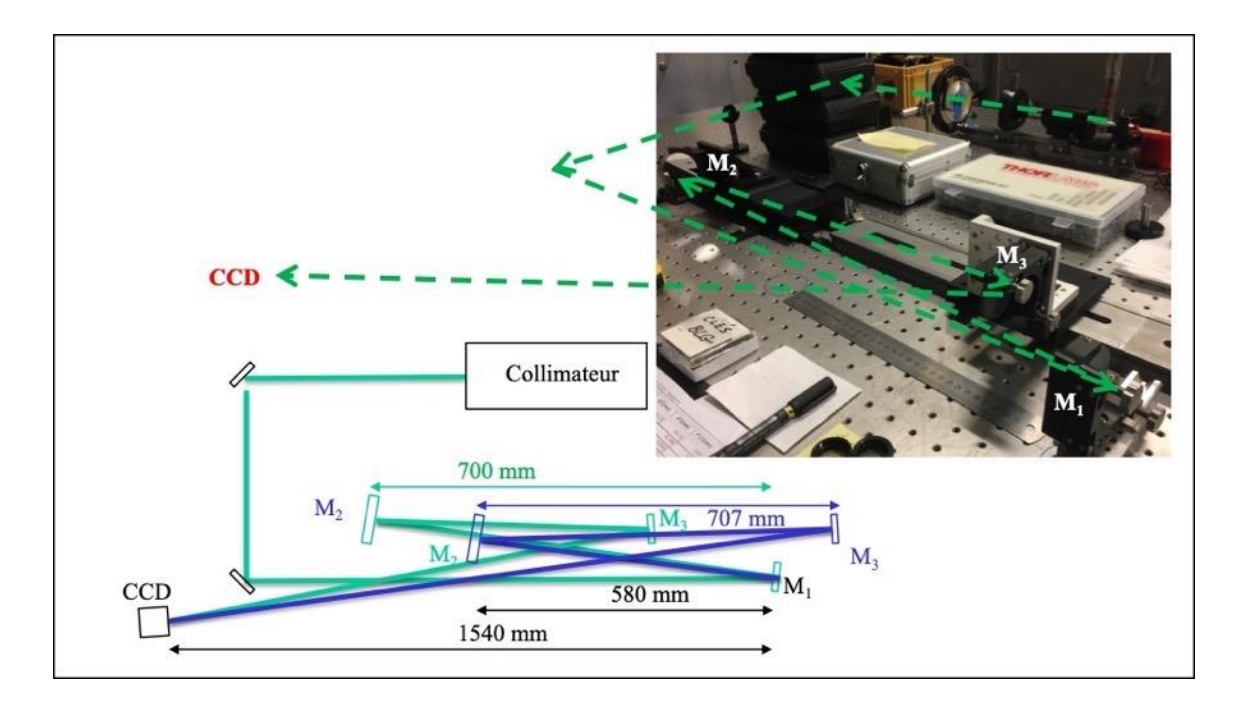


Figure 12:experimental set-up (not to scale) showing the  $3^{rd}$  zoom with the maximum range.  $M_2$  is moving 115 mm and  $M_3$  442 mm. Both translations are parallel.

For any position of  $M_2$ ,  $M_3$  is tuned such that the focal spot with minimum size is obtained on the CCD camera. Its full widths at half maximum together and its waists (according to a gaussian fit) along two transverse directions are recorded [10]. As the intensity of the focal spot increases, additional neutral densities are added (+ ND 0.6). Results are given table 3 and the corresponding focal spots are shown on figure 13.

Alignment is easy; all three mirror mounts are placed off-axis (value given from figure 7 is less than 1.7 mm and decreases as x increases) and translations for  $M_2$  and  $M_3$  are parallel to each other and to the incident beam axis. For achieving even lower off-axis, mirror mounts are cut out kinematic types (similar to Edmund Optics 50/50.8mm E-series Cut Out Kinematic Mount).

Table 3: experimental results with the  $3^{rd}$  zoom (C-C-D). Distances measured with  $\pm$  0.5 mm accuracy. Focal spots measured with  $\pm$  4  $\mu$ m accuracy. Intensity calculated over a 200- $\mu$ m diameter.

Experimental values								Calculated values		
d <sub>12</sub> (mm)	d <sub>13</sub> (mm)	FWHM x (μm)	FWHM y (μm)	FW 1/e <sup>2</sup> x (μm)	FW 1/e <sup>2</sup> y (μm)	Normalized intensity	d <sub>12</sub> (mm)	d <sub>13</sub> (mm)	f' <sub>1+2+3</sub> (mm)	
-585	127	172	164	203	193	1	-585	127	1890	
-590	97	164	158	195	190	1.054	-590	97	1790	
-607	0	139	137	166	164	1.406	-607	0	1510	
-635	-130	104	103	125	122	2.462	-635	-118	1190	
-650	-183	95	91	114	109	3.088	-650	-172	1070	
-670	-235	86	83	102	101	3.748	-670	-230	940	



-682	-273	80	76	96	92	4.366	-682	-267	870
-700	-315	72	70	87	85	5.050	-700	-315	790

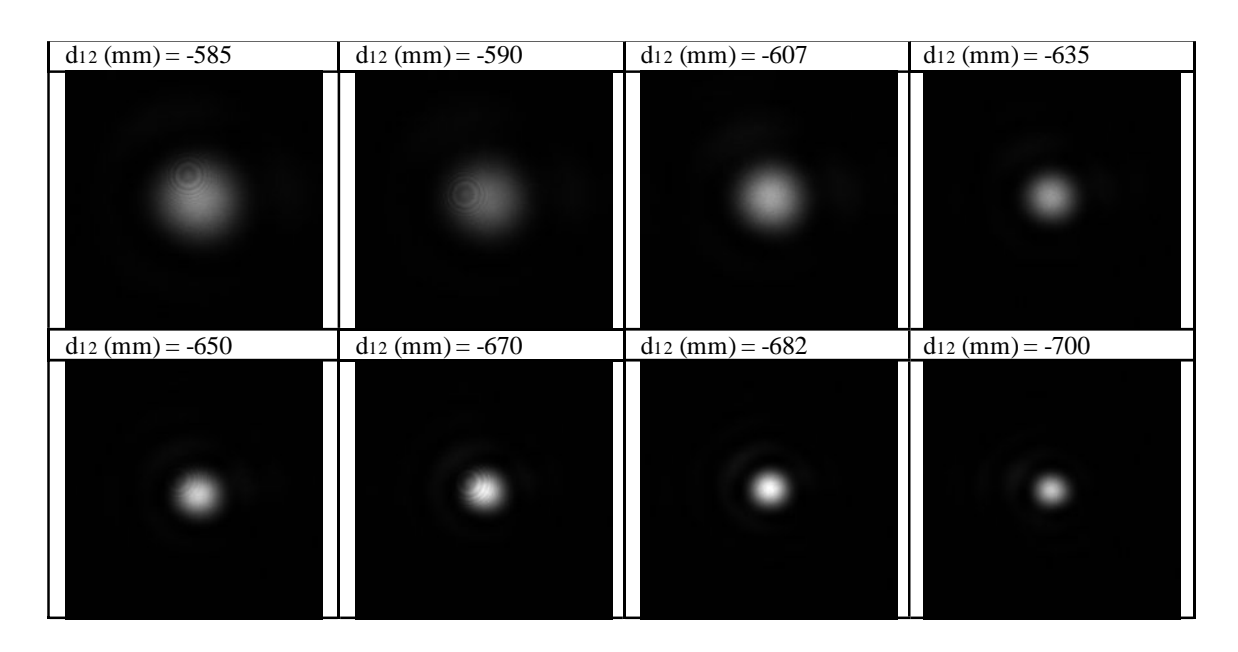


Figure 13: focal spots recorded for the 8 positions of mirrors M<sub>2</sub> and M<sub>3</sub> according to Table 3.

From these data, I can plot the square roots of the focal spot areas (at half maximum and at  $1/e^2$ ) as a function of the focal length: both are linear with a best fit with R=0.99874 and 0.99806 respectively. The plot of the normalized intensity as a function of the focal length fits a parabola with R= 0.99903.

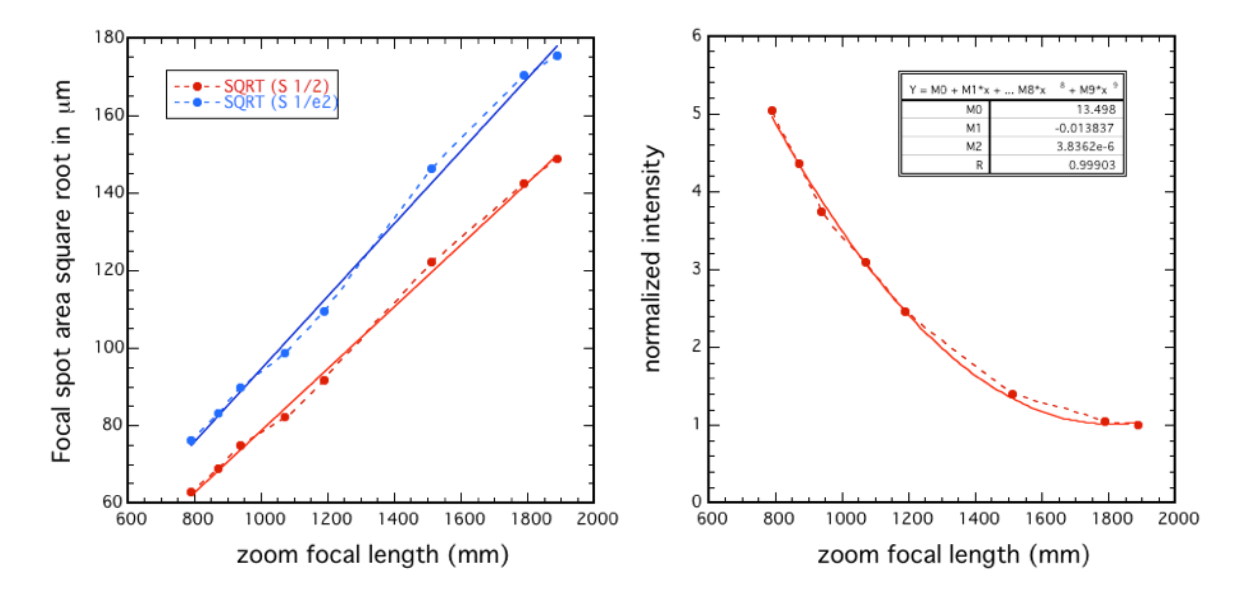


Figure 14: left, focal spot area square roots at half maximum (blue curve) and at 1/e² (red curve) as a function of the zoom focal length and right, the focal spot normalized intensity as a function of the zoom focal length.



The zoom range is 0.7 to 2.3 m focal length. At the referenced position, we have a medium range focal length of 1.56 m and a back focal length of 1.6 m. The 3 spherical mirrors are set with minimum off-axis and fit in a box less than 1 m long and 0.15 m wide. The experimental results obtained with a 8.5 mm beam excentred 6 mm show that the low wavefront distortions are not visible in the focal spot although calculations showed that the WFE is always less than 0.3 lambdas. The reason is that the remaining transverse astigmatism is always much smaller than the diffraction limit.

### 8 Conclusion

Both the size of the focal spot and the Rayleigh range of laser beams are increasing with the focal length of a focusing system. When preparing experiments for accelerating electron with lasers, people are considering focal lengths that can range from a few meters up to tens of meters. Telescopic zoom systems made of three spherical mirrors can be designed for such purpose. After a first attempt to design such system based on simple "a priori" parameters, a general algebraic theory has been investigated and shows that there are always solutions with no spherical aberration. When all mirrors are placed off-axis to avoid obscuration of the beam, it is possible to show that there are still solutions that minimize aberrations. When changing the distance between the mirrors, we can obtain a focal excursion of the system while the final focal spot is fixed. Of course, the goal of the study is to find what are the solutions that minimize aberrations for a given numerical aperture over a given zoom range. I have built and tested three zoom systems based on different solutions and I have been able to show that there are simple alignment procedures for generating a fixed focal spot over the zoom range.

Finally, while following a step-by-step approach, it has been possible to identify and compare the 4 possible configurations leading to a telescopic zoom made of three spherical mirrors. Looking at the on-axis configurations, there are five conditions that are strong limitations of the zoom range. Moreover, when going off-axis for avoiding any beam obscuration, only one configuration seems really attractive (the C-C-D configuration). At the same time and thanks to the good results I got with the reduced-scale zooms and especially with the 3rd one that confirms the high potential of the C-C-D configuration, a full-scale zoom was designed for the petawatt 140-mm F2 beam.



#### 9 References

- 1 D.N. Papadopoulos et al., "First commissioning results of the Apollon laser on the 1 PW beamline," CLEO 2019, paper Stu3E.4 (2019), <a href="https://doi.org/10.1364/CLEO\_SI.2019.STu3E.4">https://doi.org/10.1364/CLEO\_SI.2019.STu3E.4</a>
- 2 D. Korsch, "Closed-form solutions for imaging systems corrected for 3rd order aberrations", JOSA13(6) 667-672 (1973)
- 3 B. Le Garrec, "Design of a telescopic zoom system for electron acceleration with lasers", Proc. SPIE 11871, 118710R, Optical Design and Engineering VII (2021), http://dx.doi.org/10.1117/12.2597176
- 4 J. Burcher, "Les combinaisons optiques, pratique des calculs", Ed. De la Revue d'Optique Théorique et Appliquée, Paris (1967)
- 5 Born and Wolf -1980 (6th edition, chapter 5)
- 6 VirualLab Fusion version 7.0.3.4, January 2020, from LightTrans International, Kahlaische Str. 4, 07743 Jena, Germany; <a href="https://www.lighttrans.com/">https://www.lighttrans.com/</a>
- 7 Atmos Demo software 2011written by Massimo Riccardi: http://www.atmos.software.it
- 8 B. Le Garrec, "Telescopic zoom system for electron acceleration with lasers: general design and tests", Proc. SPIE 12577, 1257709, High-power, High-energy Lasers and Ultrafast Op-tical Technologies (2023), http://dx.doi.org/10.1117/12.2668426
- 9 Basler Camera acA1300-30gc: <a href="https://www.baslerweb.com/en/products/cameras/area-scan-cameras/ace/aca1300-30gc/">https://www.baslerweb.com/en/products/cameras/area-scan-cameras/ace/aca1300-30gc/</a>
- 10 Laseview software: <a href="https://en.symphotony.com/wp-content/uploads/LaseView-LHB-series-Manual-221022.pdf">https://en.symphotony.com/wp-content/uploads/LaseView-LHB-series-Manual-221022.pdf</a>